Microsc. Microanal., page 1 of 5
doi:10.1017/S1431927617012624

Microscopy AND Microanalysis

Bright-Field Microscopy of Transparent Objects: A Ray Tracing Approach

Anatoly K. Khitrin,[1,✠] Jonathan C. Petruccelli,[2] and Michael A. Model[3,*]

[1]*Department of Chemistry and Biochemistry, Kent State University, Kent, OH 44242, USA*
[2]*Department of Physics, State University of New York Albany, Albany, NY 12222, USA*
[3]*Department of Biological Sciences, Kent State University, Kent, OH 44242, USA*

Abstract: The formation of a bright-field microscopic image of a transparent phase object is described in terms of elementary geometrical optics. Our approach is based on the premise that the image replicates the intensity distribution (real or virtual) at the front focal plane of the objective. The task is therefore reduced to finding the change in intensity at the focal plane caused by the object. This can be done by ray tracing complemented with the requirement of energy conservation. Despite major simplifications involved in such an analysis, it reproduces some results from the paraxial wave theory. In addition, our analysis suggests two ways of extracting quantitative phase information from bright-field images: by vertically shifting the focal plane (the approach used in the transport-of-intensity analysis) or by varying the angle of illumination. In principle, information thus obtained should allow reconstruction of the object morphology.

Key words: Optical theory, transport-of-intensity equation, transmission microscopy, quantitative phase imaging

Introduction

The diffraction theory of image formation developed by Ernst Abbe in the 19th century remains central to understanding transmission microscopy (Born and Wolf, 1970). It has been less appreciated that certain effects in transmission imaging can be adequately described by geometrical, or ray optics. In particular, the geometrical approach is valid when one is interested in features significantly larger than the wavelength. Examples of geometrical descriptions include the explanation of Becke lines at the boundary of two media with different refractive indices (Faust, 1955) or the axial scaling effect (Visser et al., 1992). In this work, we show that a model based on geometrical optics can be used to describe the formation of a bright-field transmission image of a refractive (phase) specimen.

Our approach is based on the notion that in an infinite tube length microscope, an image replicates the real or virtual intensity distribution at the front focal plane of the objective. Thus, the effect of a refractive object can be analyzed by examining the pattern formed by extending the incoming rays back to the focal plane. Figure 1 illustrates the concept. In the absence of a specimen, the intensity distribution at the focal plane is uniform, and no image is formed. A phase specimen causes refraction of the rays, which is produces lighter and darker areas at the focal plane. These darker and lighter areas are translated into the image.

Received May 19, 2017; accepted September 25, 2017
* *Corresponding author*. mmodel@kent.edu
✠ The premature death of **Anatoly Khitrin** (1955–2017) took away from us a scientist of rare knowledge and imagination. His specialty was quantum physics and magnetic resonance, but he also had a unique ability to quickly get to the root of the most diverse problems, whether it was membrane biophysics, climate change, or trouble with a home furnace. He made original and useful inventions but never cared to patent them. Anatoly was a modest and gentle person, not seeking any special recognition, not jumping on bandwagons and "hot" topics. He thought about deep questions, achieved remarkable insights, helped colleagues and taught students – in other words, did what scientists are supposed to be doing.

Theory and Discussion

Next, we present the above model of image formation in quantitative terms. Consider a typical situation in light microscopy (Fig. 2), where an object (e.g., a biological cell) is attached to the coverglass on the side of the objective. It is illuminated by light coming from the condenser on the opposite side. The cell has a slightly higher refractive index than the surrounding liquid (typically by ~2–3%) and is assumed to have a homogeneous structure. The focal plane of a coverglass-corrected objective is positioned approximately on the level of the cells but can be shifted up or down by moving either the sample or the objective.

Figure 3 gives a more detailed view of the ray path through the sample. A single refraction at the interface of the cell and its aqueous environment is assumed. It causes a change in the distribution of intensity at the focal plane of the objective, which, in turn, determines the intensity distribution at the image plane. It is possible, of course, to have a situation when the focal plane is below the cell, in which case the intensity would also be affected by a second refraction at the cell-coverglass boundary. This case will not be considered.

Figure 3 introduces the main parameters used in the model. From the law of refraction, we have:

$$\frac{\sin\alpha}{\sin\beta} = \frac{n_2}{n_1} = n, \qquad (1)$$

where n is the relative refractive index. To simplify the following derivations, we assume that $n-1 \ll 1$, which is

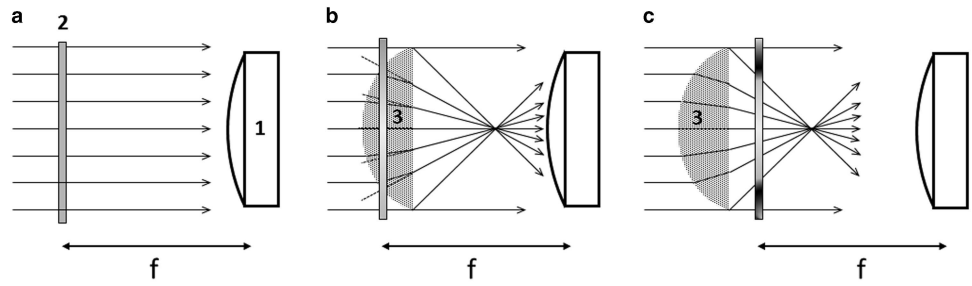

Figure 1. In the absence of a specimen, a uniform illumination at the focal plane (2) of the objective (1) produces no contrast (**a**). The refractive specimen (3), which, for the sake of simplicity, is depicted here as a lens, alters the distribution of intensity at the focal plane of the objective; the latter may lie inside (**b**) or outside (**c**) the sample. The intensity pattern at the focal plane is reproduced by the optical system and generates an image. In the case (**b**), one expects a lighter area in the central part, where the density of back-projected rays is higher. In the case (**c**), the area immediately outside the cone of light formed by the specimen is completely dark. (This effect can be easily observed by putting a lens under the microscope.)

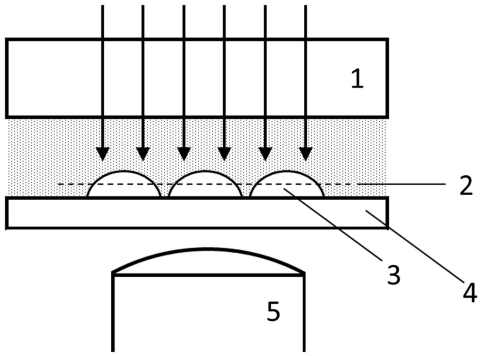

Figure 2. General setup in transmission brightfield imaging. 1, —slide; 2, focal plane; 3, object; 4, coverglass; 5, objective.

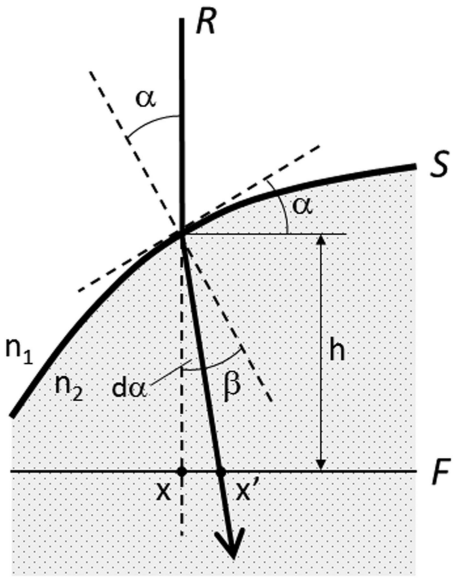

Figure 3. The diagram of rays crossing the sample. A vertical incident ray R impinges on the object boundary S at the angle α. Refraction causes its deflection from the vertical line by $d\alpha$. The point of intersection of R and S lies at the distance h from the focal plane F. As a result, the point where the R ray crosses the focal plane F shifts from x to x'. The focal plane is designated as xy, and the refraction takes place in the xz-plane.

usually true for live biological cells. Then, the angle of refraction $d\alpha = \alpha - \beta$ is small, and Equation (1) can be written as:

$$\frac{\sin\alpha}{\sin(\alpha - d\alpha)} = \frac{\sin\alpha}{\sin\alpha - d\sin\alpha} = \frac{\sin\alpha}{\sin\alpha - d\alpha\cos\alpha} = \frac{1}{1 - d\alpha / \tan\alpha} = n. \tag{2}$$

From here we find the refraction angle:

$$d\alpha = (n-1)\tan\alpha = (n-1)\frac{dh(x)}{dx}, \tag{3}$$

where $h(x)$ is the height of the object boundary over the focal plane (it can be positive or negative), and x is the position on the focal plane where it would be intersected by the incident ray in the absence of the sample. Refraction causes a shift of the intersection point from x to x'. For small refraction angles $d\alpha$:

$$x' = x + h(x)d\alpha = x + h(x)(n-1)\frac{dh(x)}{dx}. \tag{4}$$

Image intensity $I(x')$ satisfies the equation:

$$I(x')dx' = I_0(x)dx, \tag{5}$$

where $I_0(x)$ is the incident light intensity. Equation (5) states the condition of energy conservation: all the incident rays that would arrive at the element dx without refraction are deflected to the element dx' in the presence of refraction. If we assume uniform illumination and use relative intensities, we can set $I_0(x) = 1$. Then:

$$I(x') = \frac{dx}{dx'} = \frac{1}{dx'/dx}, \tag{6}$$

or, taking Equation (4) into account:

$$\begin{aligned} I(x') &= \left[1 + (n-1)\left\{h(x)\frac{d^2h(x)}{dx^2} + \left(\frac{dh(x)}{dx}\right)^2\right\}\right]^{-1} \\ &= \left[1 + (n-1)\frac{d}{dx}\left\{h(x)\frac{dh(x)}{dx}\right\}\right]^{-1} \\ &= \left[1 + \frac{(n-1)}{2}\frac{d^2\{h^2(x)\}}{dx^2}\right]^{-1}. \end{aligned} \tag{7}$$

Two-dimensional (2D) generalization can be done as follows. By analogy with Equation (4), the position vector (x',y') on the focal plane, where the continuation of refracted rays crosses the focal plane, can be written as:

$$(x', y') = (x, y) + h(x, y)(n-1)\nabla h(x, y), \tag{8}$$

where ∇ is the 2D gradient in the *xy*-plane. In terms of the components:

$$x' = x + h(x, y)(n-1)\frac{\partial h(x, y)}{\partial x}, y' = y + h(x, y)(n-1)\frac{\partial h(x, y)}{\partial y}. \tag{9}$$

The line elements *dx* and *dx*' in Equation (6) have to be replaced by the area elements *dxdy* and *dx'dy'*, and the equivalent of Equation (6) takes the form:

$$I^{-1}(x', y') = \left|\frac{\partial(x', y')}{\partial(x, y)}\right|. \tag{10}$$

Thus, the inverse intensity of the image is the Jacobian determinant $\left|\frac{\partial(x', y')}{\partial(x, y)}\right|$. By substituting *x*' and *y*' from Equation (9), one obtains:

$$\begin{aligned} \mathrm{I}^{-1}(x', y') = \frac{\partial x'}{\partial x}\frac{\partial y'}{\partial y} - \frac{\partial y'}{\partial x}\frac{\partial x'}{\partial y} = \left[1 + (n-1)\left\{h\frac{\partial^2 h}{\partial x^2} + \left(\frac{\partial h}{\mathrm{d}x}\right)^2\right\}\right] \cdot \\ \left[1 + (n-1)\left\{h\frac{\partial^2 h}{\partial y^2} + \left(\frac{\partial h}{dy}\right)^2\right\}\right] \\ - \left[(n-1)\left(h\frac{\partial^2 h}{\partial x \partial y} + \frac{\partial h}{dx}\frac{\partial h}{dy}\right)\right]^2. \end{aligned} \tag{11}$$

This equation can be simplified if we assume that variations of the image intensity are small compared with the average intensity. Then:

$$\begin{aligned} I^{-1}(x', y') &= 1 + (n-1)\left\{h\left(\frac{\partial^2 h}{\partial x^2} + \frac{\partial^2 h}{\partial y^2}\right) + \left(\frac{\partial h}{\mathrm{d}x}\right)^2 + \left(\frac{\partial h}{dy}\right)^2\right\} \\ &= 1 + (n-1)\nabla \cdot \{h(x, y)\nabla h(x, y)\} \\ &= 1 + \frac{n-1}{2}\nabla^2 h^2(x, y), \end{aligned} \tag{12}$$

where ∇^2 denotes the 2D Laplacian in the *xy*-plane. This can be viewed as a general equation for image intensity. It can be readily rearranged as a Poisson's equation for object height *h* in terms of known quantities (measured intensity and refractive index) as:

$$\frac{2}{n-1}\left[I^{-1}(x', y') - 1\right] = \nabla^2 h^2(x, y), \tag{13}$$

which can be solved uniquely for h^2 provided boundary conditions on h^2 are supplied. Equation (13) has a strikingly similar form to the transport-of-intensity equation (TIE), which will be discussed in the following section, in that the measured intensity for a pure-phase object is related to a function of the sample's thickness through a Poisson's equation. Therefore, many of the techniques developed for solving the TIE may be applicable to this model as well (Paganin and Nugent, 1998; Volkov et al., 2002; Bardsley et al., 2011; Tian et al, 2012; Kostenko et al., 2013; Martinez-Carranza, et al., 2013).

To create a more easily interpretable contrast, one can collect several images taken under slightly different conditions:

(1) Shift of the focal plane

A shift of the focal plane by *dz* corresponds to the substitution $h(x,y) \to h(x,y) - dz$ in Equation (12) and has no effect on the derivatives. Therefore, one can construct the difference:

$$I_2^{-1}(x', y') - I_1^{-1}(x', y') = -dz(n-1)\nabla^2 h(x, y), \tag{14}$$

where I_1 and I_2 are the image intensities at two different positions of the focal plane. Now Equation (14) has a simple interpretation: the contrast is proportional to the local curvature of the object boundary. This is a well-known fact, used, for example, in "defocusing" microscopy (Agero et al., 2004).

It is interesting to compare this result with TIE (Teague, 1983; Streibl, 1984) obtained from the paraxial wave equation. The TIE equation for the "logarithmic derivative" [Equation (7b) in Streibl, 1984 at uniform transmittance] is:

$$\left(\frac{d}{dz}\right)\ln I(x, y; z = 0) = -\nabla^2 \varphi(x, y), \tag{15}$$

where $\varphi(x,y)$ is the phase. If we use a low-contrast approximation [as in Equation (12)] and realize that $(n-1)h(x,y)$ is equivalent to the phase $\phi(x,y)$, then Equations (14) and (15) become identical. Both are the Poisson equations for the object profile $h(x,y)$, where the left side represents experimental data. In the presence of image noise and for objects with complex shape, this equation is difficult to solve. Indeed, by applying the 2D Gauss theorem, one can see that perturbation from a noisy pixel does not decay, but grows logarithmically with the distance from the pixel. Within the TIE approach, various computational methods have been developed to minimize artifacts in restored phase maps (Volkov et al., 2002; Waller et al., 2010; Bardsley et al., 2011; Bie et al., 2012; Tian et al., 2012; Zheng et al., 2012; Kostenko et al., 2013; Petruccelli et al., 2013; Zuo et al., 2013; Jingshan et al., 2014).

Note that although both Equations (13) and (14) are Poisson's equations, they are based on two different mechanisms of contrast generation. In both cases, it is propagation of refracted rays that generates measurable intensity contrast, where refraction depends on variations in the object's height h. In the case of Equation (13), propagation is through the object itself, which is why the Poisson's equation depends on the square of object height. In Equation (14), defocus by an amount *dz* is used to generate the contrast so the Poisson's equation depends on the product of *dz* and the object height.

In the practical realization of the vertical shift method, two additional considerations apply. First, the vertical shift of the focal plane is not equivalent to the vertical shift of the objective (or of the stage), which is the only distance reported by the microscope hardware. Thus, to obtain the true *dz* to be

used in the calculations, the nominal shift must be multiplied by the ratio of n_1 (or n_2, as they are nearly equal) to the refractive index of the immersion medium of the objective (Carlsson, 1991; Visser et al., 1992). Second, the focal plane must remain within the sample or the medium, but not within the coverglass, as that would introduce a second refraction which is not accounted for by Equation (14). For example, if the first image is focused on the coverglass surface, the second or subsequent images should be focused further into the sample.

(2) Varying the illumination angle

The other way of creating an interpretable contrast is to vary the illumination angle, for example, by using an off-center condenser diaphragm. Variable angle illumination has been used in differential phase contrast microscopy (Hamilton and Sheppard, 1984; Tian and Waller, 2015; Chen et al, 2016) and computer tomography (Sung et al, 2009). Here we show that quantitative data can, in principle, be extracted from the above ray model. If γ_x and γ_y are small tilt angles in the xz- and yz-planes, one can use two pairs of images, taken at $\pm\gamma$. For the angle γ, Equation (3) is modified as:

$$d\alpha = (n-1)\tan(\alpha+\gamma) = (n-1)\frac{\tan\alpha+\tan\gamma}{1-\tan\alpha\tan\gamma}$$
$$\approx (n-1)\frac{\tan\alpha+\gamma}{1-\gamma\tan\alpha}. \qquad (16)$$

At $\gamma\tan\alpha \ll 1$, the difference between each pair of images can be expressed as:

$$I^{-1}_{+\gamma x}(x',y') - I^{-1}_{-\gamma x}(x',y') = 4\gamma_x(n-1)\frac{\partial h}{\partial x}\left[1+\left(\frac{\partial h}{\partial x}\right)^2\right],$$
$$I^{-1}_{+\gamma y}(x',y') - I^{-1}_{-\gamma y}(x',y') = 4\gamma_y(n-1)\frac{\partial h}{\partial y}\left[1+\left(\frac{\partial h}{\partial y}\right)^2\right]. \qquad (17)$$

These are algebraic equations for $\frac{\partial h}{\partial x}$ and $\frac{\partial h}{\partial y}$. When the derivatives are not too large, the contrast essentially represents the slope of the profile $h(x,y)$ along the corresponding direction. After the derivatives are found, the profile $h(x,y)$ can be obtained by simple integration. However, one complication might arise if one strives for a higher resolution. The images forming each pair in Equation (17) are misregistered by the amount $\gamma h(x,y)$. This would make the task of numerical reconstruction of the profile $h(x,y)$ at high resolution less straightforward.

In summary, we have presented a simple theory of transmission image formation based on ray tracing. The theory relates directly to the quantity of interest—the object profile. If the profile of a cell is known from independent measurements, one should be able to find the average refractive index, as well as related quantities—water and protein concentration. Local protein/water variations are usually less important than the integral values over the entire cell volume, and thus the geometrical description is appropriate. Although ray tracing is a very simplified description of light propagation, our results are equivalent to those based on paraxial wave theory (Teague, 1983; Streibl, 1984). The other finding is the possibility of extracting quantitative phase information from variable illumination angle, which leads to simpler equations. Future work will test the practicality of this approach.

Acknowledgments

The research was supported by the ACS Petroleum Research Fund 58813-ND6 to A.K.K. and the University Research Council Grant to M.A.M.

References

Agero, U., Mesquita, L.G., Neves, B.R., Gazzinelli, R.T. & Mesquita, O.N. (2004). Defocusing microscopy. *Microsc Res Tech* **65**, 159–165.

Bardsley, J. M., Knepper, S. & Nagy, J. (2011). Structured linear algebra problems in adaptive optics imaging. *Adv Comput Math* **35**, 103–117.

Bie, R., Yuan, X.H., Zhao, M. & Zhang, L. (2012). Method for estimating the axial intensity derivative in the TIE with higher order intensity derivatives and noise suppression. *Opt Express* **20**, 8186.

Born, M. & Wolf, E. (1970). *Principles of Optics*, 4th ed. Oxford: Pergamon Press.

Carlsson, K. (1991). The influence of specimen refractive index, detector signal integration, and non-uniform scan speed on the imaging properties in confocal microscopy. *J Microsc* **163**, 167–178.

Chen, M., Tian, L. & Waller, L. (2016). 3D differential phase contrast microscopy. *Biomed Opt Express* **7**, 3940–3950.

Faust, R.C. (1955). Refractive index determinations by the central illumination (Becke line) method. *Proc Phys Soc B* **68**, 1081.

Hamilton, D.K. & Sheppard, C.J.R. (1984). Differential phase contrast in scanning optical microscopy. *J Microsc* **133**, 27–39.

Jingshan, Z., Claus, R.A., Dauwels, J., Tian, L. & Waller, L (2014). Transport of Intensity phase imaging y intensity spectrum fitting of exponentially spaced defocus planes. *Opt Express* **22**, 18125–18137.

Kostenko, A., Batenburg, K.J., Suhonen, H., Offerman, S.E. & van Vliet, L.J. (2013). Phase retrieval in in-line x-ray phase contrast imaging based on total variation minimization. *Opt Express* **21**, 710–723.

Martinez-Carranza, J., Falaggis, K., Kozacki, T. & Kujawinska, M (2013). Effect of imposed boundary conditions on the accuracy of transport of intensity equation based solvers. *Proc SPIE* **8789**, 87890N.

Paganin, D. & Nugent, K.A. (1998). Noninterferometric phase imaging with partially coherent light. *Phys Rev Lett* **80**, 2586–2589.

Petruccelli, J.C., Tian, L. & Barbastathis, G. (2013). The transport of intensity equation for optical path length recovery using partially coherent illumination. *Opt Express* **21**, 14430–14441.

Streibl, N. (1984). Phase imaging by the transport equation of intensity. *Opt Commun* **49**, 6–10.

Sung, Y., Choi, W., Fang-Yen, C., Badizadegan, K., Dasari, R.R. & Feld, M.S. (2009). Optical diffraction tomography for high resolution live cell imaging. *Opt Express* **17**, 266–277.

Tian, L., Petruccelli, J.C. & Barbastathis, G. (2012). Nonlinear diffusion regularization for transport of intensity phase imaging. *Opt Lett* **37**, 4131–4133.

Tian, L. & Waller, L. (2015). 3D intensity and phase imaging from light field measurements in an LED array microscope. *Optica* **2**, 104–111.

Teague, M.R. (1983). Deterministic phase retrieval: A Green's function solution. *J Opt Soc Am* **73**, 1434–1441.

Visser, T.D., Oud, J.L. & Brakenhoff, G.J. (1992). Refractive index and axial distance measurements in 3-D microscopy. *Optik* **90**, 17–19.

Volkov, V.V., Zhu, Y. & De Graef, M. (2002). A new symmetrized solution for phase retrieval using the transport of intensity equation. *Micron* **33**, 411–416.

Waller, L., Tian, L. & Barbastathis, G. (2010). Transport of Intensity phase-amplitude imaging with higher order intensity derivatives. *Opt Express* **18**, 12552–12561.

Zheng, S., Xue, B., Xue, W., Bai, X. & Zhou, F. (2012). Transport of intensity phase imaging from multiple noisy intensities measured in unequally spaced planes. *Opt Express* **20**, 972.

Zuo, C., Chen, Q., Yu, Y. & Asundi, A. (2013). Transport-of-intensity phase imaging using Savitzky-Golay differentiation filter–theory and applications. *Opt Express* **21**, 5346–5362.